Journal of Energy Storage 67 (2023) 107615

Contents lists available at ScienceDirect

Journal of Energy Storage

journal homepage: www.elsevier.com/locate/est

Research papers

Synthesis of polyaniline-graphene oxide based ternary nanocomposite for supercapacitor application

Md Mostafizur Rahman [a,d,*], Minhazur Rahman Shawon [a], Md Habibur Rahman [a], Iftidul Alam [a], Muhammad Omar Faruk [b], Mohammad Mizanur Rahman Khan [c], Okenwa Okoli [d]

[a] *Department of Chemical Engineering and Polymer Science, Shahjalal University of Science and Technology (SUST), Sylhet 3114, Bangladesh*
[b] *Department of Physics, SUST, Sylhet 3114, Bangladesh*
[c] *Department of Chemistry, SUST, Sylhet 3114, Bangladesh*
[d] *Herff College of Engineering, University of Memphis, Memphis, TN 38152, USA*

ARTICLE INFO

Keywords:
Synthesis
Graphene oxide
Ternary nanocomposite
Supercapacitor
Device performance

ABSTRACT

This study focuses on the synthesis of Polyaniline (PANI), graphene oxide (GO), and their nanocomposites with metal oxides (MO) and hexagonal boron nitride (h-BN) for their application in the supercapacitor. In this study, PANI/GO, PANI/GO/TiO_2, PANI/GO/MoS_2 and PANI/GO/h-BN ternary nanocomposites were synthesized following a chemical oxidative polymerization method. The prepared nanocomposites were characterized by FTIR, XRD, TGA, SEM and electrochemical analysis. The electrochemical properties of the nanocomposites were evaluated by cyclic voltammetry (CV), galvanostatic charge-discharge (GCD), electrochemical polarization and impedance analysis. CV profile of the nanocomposite showed that incorporation of GO, MO and h-BN in the polyaniline backbone improved capacitance, energy density and power density significantly. Among the synthesized ternary nanocomposites, PANI/GO/h-BN showed highest capacitance of 946 F/g and high capacitance retention after 100 cycles of charging and discharging. Finally, a set of hybrid asymmetric supercapacitors were constructed using the synthesized nanocomposites as positive electrode and activated carbon as negative electrode. The device was assessed following the GCD method. The supercapacitor device with PANI/GO/h-BN nanocomposite as positive electrode exhibited higher specific capacitance of 351 F/g with high power density of 4500 W/kg, and it lit up a 5 mm LED for 243 min, indicating its superiority over other electrodes.

1. Introduction

Conductive polymer composites (CPC) have been fostered in many widespread applications due to their unique electrochemical properties [1]. CPC has been considered as a hotspot for research as electrode materials for supercapacitors because of their high electrochemical properties and charge storage capacity [2]. CPC-based electrodes can undergo a quick and reversible redox reaction, allowing them to store high-density charges and produce large faradic capacitances [3,4]. However, conducting polymers may swell and shrink during the electrochemical redox process that result in limited cycle life [5,6]. As a result, improvement in the cyclic stability of CPC electrodes has become a burning issue. In general, conductive polymer composites prepared with a combination of carbonaceous material, metal oxides, metal hydroxides, or metal sulfides can buffer volume change during repeated redox cycles while also improving mechanical stability and specific capacitance [7,8].

For example, PANI has weak structure and poor performance in counter ion insertion/deinsertion and charge/discharge cycle life, and thus PANI needs to be combined with advanced materials for high-technology applications. On the other hand, carbonaceous materials (e.g. Graphene, GO, CNT etc.) have good structural stability, better electrical properties, large surface area, high electron mobility, and mechanical/thermal stability. Thus, graphene in combination with PANI has great potential as an electrode for supercapacitor, and has been utilized in various applications [9]. PANI has less electrical conductivity property due to dopant migration (e.g., HCl is a small molecule that migrates to the surface over time).

The combination of GO and PANI exhibits an attractive character in comparison with pristine PANI. However, PANI/GO composites provide

---

* Corresponding author at: Department of Chemical Engineering and Polymer Science, Shahjalal University of Science and Technology (SUST), Sylhet 3114, Bangladesh.

E-mail address: mostafizur.cep@gmail.com (M.M. Rahman).

https://doi.org/10.1016/j.est.2023.107615
Received 4 February 2023; Received in revised form 14 April 2023; Accepted 2 May 2023

better conductivity as GO is acidic in nature, remains conductive for a long time, and no migration occurs in composites. PANI/GO composites show better electro activity due to synergistic effects of PANI and GO [10]. Wang et al. prepared layered GO doped PANI for supercapacitor applications by in situ polymerization of aniline in the presence of graphene oxide [10].

Zhang et al. reported that incorporation of graphene with PANI significantly improved the chemical structure and electrochemical properties of the composite, and PANI/GO composites showed specific capacitance of 480 F/g [11]. Similarly, Mao et al. prepared PANI/GO nanocomposites by in-situ polymerization, and used as electrode for supercapacitors, the PANI/GO electrode demonstrated good electrochemical performance with a specific capacitance of 526 F/g [12]. Wang et al. (2020) reported that p-Phenylenediamine (PPD) incorporated PANI/rGO composite showed excellent supercapacitor performance due to superior electrochemical properties of GO and the synergistic effect of PPD-rGO and PANI [13]. PANI/PPD-rGO composites exhibited specific capacitance of 635.2 F/g at a current density of 1 A/g. Zhou et al. prepared graphene-wrapped polyaniline nanofibers as electrodes for supercapacitors [14].

Zhang et al. synthesized PANI/GO composite for supercapacitor by an electro-polymerization approach [15]. The composite film with a graphene oxide content of 10 mg/l showed maximum specific capacitance of 1136.4 F/g, which was nearly two-fold higher than that of polyaniline.

It is also reported that compounding of transition metal oxide such as ZnO, TiO_2 powder and CdS with GO can effectively enhance the electrochemical performance of the composite [5,8]. A number of studies in the literature show that a combination of metal oxides, carbonaceous materials, 2D materials such as graphene, Boron nitride (BN), transition metal dichalcogenides, and other materials with PANI improves electrochemical performance of the CPC [16,17].

Although some studies have been reported on PANI/GO composite as electrode materials, most of the studies have only focused on potentiostatic performance of electrode materials, and construction of supercapacitor cell and device performance were less discussed in the literature. Electrochemical studies in a three-electrode system cannot assess actual performance of an electrode because three electrode systems can measure potential change only on a working electrode with respect to reference electrodes. Therefore, fabrication of a real supercapacitor device and measuring of its performance galvanostatically in two electrode systems is very crucial. In fact, for the complete assessment of an electrode material, it is essential to evaluate the electrode by all three configurations (potentiostatic, galvanostatic and real device performance). However, in many previous studies, electrode materials and device performances are not explored systematically.

As such in this study, GO was synthesized from graphite following modified Hummer's method, and then PANI/GO, PANI/GO/h-BN, PANI/GO/TiO_2, PANI/GO/MoS_2 ternary nanocomposites were synthesized and characterized systematically by FTIR, XRD, TGA, SEM and electrochemical analysis. Electrochemical properties of the synthesized composites were evaluated by GCD, cyclic voltammetry, electrochemical polarization and impedance analysis using an electrochemical workstation. Electrochemical performance of the electrode materials determined by CV study were supported by impedance analysis. Finally, a set of asymmetric hybrid supercapacitors were constructed using the synthesized nanocomposite materials as positive electrode, and the performance of the supercapacitor was evaluated galvanostatically in a two-electrode system using a DC load bank at constant current. In fact, electrode materials and supercapacitor device developed in this study were evaluated properly by all three configurations (i.e. potentiostatic, galvanostatic and real device performances).

2. Materials and methods

2.1. Materials

For the synthesis of graphene oxide from graphite powder, hydrogen peroxide (H_2O_2), concentrated sulphuric acid (H_2SO_4), potassium permanganate ($KMnO_4$) was used. Aniline 99 % (Alfa Aesar, UK), Ammonium peroxydisulfate (APS) (PT. Smart Lab, Indonesia) and Hydrochloric acid 37 % (Merck, Germany) were collected and used for synthesis of PANI. In addition, hexagonal boron nitride (h-BN) was collected from BORTEK, Turkey and used for the synthesis of PANI/GO/h-BN composites. The purity of nano h-BN was 99.97 %. The particle size of h-BN ranged 0.01–1.16 μm, and sp. surface area of h-BN was 29.8 m^2/g. Titanium dioxide (TiO_2) and Molybdenum sulfide (MoS_2) were used for the synthesis of PANI/GO/TiO_2 and PANI/GO/MoS_2 nanocomposites, respectively.

2.2. Methods

2.2.1. Synthesis of graphene oxide

Graphene oxide was synthesized from graphite following a modified hummers method. 1 g of graphite flax was grinded and the graphite powder was dissolved in sufficient amounts of 1 M concentrated sulphuric acid in a water bath with continuous stirring keeping the temperature low. Then, 3 g potassium permanganate and 0.075 g sodium nitrate were added into the solution while continuous stirring. The solution was stirred continuously for 2 h in an ice bath and a small amount of deionized water was added carefully. The ice bath was removed, then the solution was heated to 90 °C for 30 mins. Finally, 20 ml hydrogen peroxide and 100 ml deionized water was added carefully to stop the reaction and a yellow-colored solution was formed after the addition of hydrogen peroxide. The solution was taken in a high-speed centrifuge (5000 rpm) for 30 min to separate the graphene oxide from the solution. The remaining solution was filtered and dried in an oven at 60 °C for 24 h and the powder obtained was graphene oxide.

2.2.2. Synthesis of PANI and PANI/GO nanocomposite

For PANI, aniline monomer was dissolved into 1 M HCl solution, and 0.8 M acidic APS solution was added dropwise into the aniline solution at 0–5 °C with continuous stirring for 6 h to continue the polymerization reactions. Subsequently, 10 ml of acetone was mixed into the above reaction mixture to control the growth of the PANI. Then, the obtained product was filtered, repeatedly washed with DI water, and dried in a freeze dryer.

In case of PANI/GO synthesis, 2 % of GO solution in 1 M concentrated Hydrochloric acid solution was prepared and the solution was sonicated for 2 h at 25 °C temperature. The dispersed solutions were mixed with 0.2 M aniline solution and stirred in a magnetic stirrer for 1 h. Then, 0.8 M acidic APS solution was added dropwise into the mixture of aniline solution and GO dispersion at 0–5 °C with continuous stirring for 6 h to continue the polymerization reaction. Subsequently, 10 ml of acetone were mixed into the mixtures to control the growth of the PANI. Thereafter similar steps were followed as for synthesis of PANI.

2.2.3. Synthesis of PANI/GO/h-BN, PANI/GO/TiO_2 and PANI/GO/MoS_2 ternary nanocomposites

Calculated amounts of GO and h-BN were dispersed in 1 M concentrated Hydrochloric acid for 2 h at 25 °C temperature using an ultrasonic bath. The dispersed solutions were mixed with 0.2 M aniline solution and stirred in a magnetic stirrer for 1 h. Then, 0.8 M acidic APS solution was added dropwise into the mixture at 0–5 °C with continuous stirring for 6 h to continue the polymerization reaction. Subsequently, 10 ml of acetone was mixed into the mixtures to control the reaction. Thereafter, similar steps were followed as for the synthesis of PANI/GO.

PANI/GO/MoS_2 and PANI/GO-TiO_2 nanocomposite was synthesized using MoS_2 and TiO_2, respectively following similar steps as followed for the synthesis of PANI/GO/h-BN nanocomposite.

2.2.4. Characterization of the samples

The chemical structures of the synthesized nanocomposite samples were analyzed by the Fourier transform infrared (FTIR) spectroscopy (Shimadzu, IRSpirit-T, Japan). The crystal structures of the samples were investigated by X-ray diffraction (XRD) patterns using a diffractometer (Rigaku SmartLab) with a Cu-K$_\alpha$ radiation source (λ = 0.154060 nm). The thermogravimetric analysis device (Shimadzu, TGA 50, Japan) was used to study the thermal stability of the synthesized composite. The Wayne Kerr 6500B impedance analyzer was used to measure dielectric loss and Impedance data. The surface morphology of the synthesized materials was studied using a scanning electron microscope (JEOL, JSM-7600 F, Japan).

2.2.5. Electrochemical measurements of electrodes

Electrochemical characteristics of all the synthesized electrode materials were pursued using potentiostat workstation (CS 105). 1 M Na_2SO_4 was used as an electrolyte and electrochemical cell with a three-electrode system (Ag/ AgCl as reference, platinum wire as counter electrode and glassy carbon electrode as working electrode). The active mass of the working electrode was found to be 1.1 mg. The Faraday reaction was investigated by CV between the wide potential of −0.3 to +0.8 V. The charge/discharge capability was tested by a GCD technique.

2.2.6. Construction of asymmetric supercapacitor device (ASD)

Based on the excellent electrochemical performance of nanocomposites in the three-electrode system, a set of hybrid asymmetric supercapacitors was assembled using the prepared nanocomposite as positive electrode and activated carbon (AC) material as negative electrode. The ASD was fabricated with binary electrode sections consisting of anode and cathode materials separated with a microporous separator. The whole system was squeezed between two current collectors which functioned as terminals while charging and discharging [16]. Copper sheet of 0.5 mm thickness was used as the current collector in this study. The current collectors work as a transporting medium of current from current source to the electrode, and electrode to external load. The synthesized composite material was mixed with cobalt oxide and APS and pasted onto the current collector by brush. On the other hand, AC was mixed with electrolyte (1 M Sodium sulfate solution), and pasted onto another current collector by brush (supplementary Fig. S1A). Thereafter the electrode was left to dry properly. Then the separator was placed between the electrodes and Na_2SO_4 (1 M) was added dropwise. After preparing the cell, the whole setup was connected with a DC power supply for charging at a constant voltage of 4 V, and also connected with the DC load bank for galvanostatic charge-discharge (Fig. S1B). The performance of the supercapacitor was evaluated based on discharge time specific capacitance, energy density and power density, cyclic retention and coulombic efficiency.

2.2.7. Devices performances evaluation

The constructed supercapacitor device was charged using DC power supply at a constant current, and it was discharged Galvanostatically using a DC load bank at constant current. Capacitance, energy density, power density, coulombic efficiency and cyclic retention was calculated following the Eqs. (1), (2), (3), (4) and (5) respectively.

$$C = \frac{It}{m\Delta V} \tag{1}$$

where C denotes capacitance in F/g, I represent current, t indicates discharge time in second, ΔV denotes voltage difference, m is the weight of materials. I, t and ΔV were found from the DC load bank, and sp. Capacitance was calculated following Eq. (1).

$$E = \frac{1}{2}CV^2 \tag{2}$$

where E stands for the energy density (Wh/kg), and V stands for voltage. Power density (W/kg) is calculated following the Eq. (3).

$$P = \frac{E}{t} \tag{3}$$

The coulombic efficiency of supercapacitor is calculated by the equation

$$\mathrm{CE} = \frac{Q_d}{Q_c} = \frac{I_{disscharge} \times t_{discharge}}{I_{charge} \times t_{charge}} \tag{4}$$

where, Q represents the amount of charge, or capacity. For constant current operation Q = It. Where I represent current and t represents time.

Cyclic retention of supercapacitor is calculated by this equation

$$\text{Cyclic retention\%after n}^{\text{th}}\text{ cycle} = \frac{Specific\ capacitance\ at\ n^{th}\ cycle}{Specific\ capacitance\ at\ 1^{st} cycle} \times 100 \tag{5}$$

Similar methods were also followed in the previous studies [16,19].

3. Results and discussion

3.1. FTIR spectroscopy study

FTIR spectra of the GO, PANI, PANI/GO, PANI/GO/MoS_2, PANI/GO/h-BN, PANI/GO/TiO_2 nanocomposites are presented in Fig. 1. The peaks identified at 3410–3430 cm^{-1} for all samples are assigned to the stretching vibrations of –OH groups, which may be from adsorbed water molecules, phenolic OH, or OH from carboxylic groups [20].

As can be seen from Fig. 1 (a), the spectrum of GO showed the peaks at 1430 and 1050 cm^{-1} are assigned to asymmetric –COOH stretching vibration, and stretching of C—O bond, respectively [20]. The other peaks observed at 815 cm^{-1} corresponds to vibrational modes of epoxide (C–O–C), 1210 cm^{-1} is assigned to epoxide and hydroxyl (C–O–C and C–OH), and 1620, 1740 cm^{-1} are designed to ketone (C=O). All of these characteristic peaks indicate the successful grafting of epoxide, hydroxyl, and carboxyl functional groups on the graphite powers to form GO through the oxidation reaction. The existence of PANI can be confirmed (Fig. 1) from the characteristic peaks of C=N and C=H stretching vibration of quinoid (Q) and benzenoid (B) skeletons at 1580 and 1480 cm^{-1}, respectively and signals at 1310 and 804 cm^{-1} that are associated with C—N and bending C—H (out of plane) stretching of benzene, respectively. The band at 1110 cm^{-1} belongs to N = Q = N and the broad signal at 3456 cm^{-1} is contributed to the N—H stretching [7].

It is obvious from the spectra that the PANI/GO composites contain the majority of the characteristic peaks of PANI and GO. These results confirmed that the GO are incorporated with PANI. Further, the characteristic N—H stretching vibration peak of PANI along with other characteristic peaks of both PANI and GO are shifted for all the composite samples synthesized by the addition of MoS_2, h-BN, and TiO_2, respectively as presented in Fig. 1. Such shifting of the peaks indicates the successful formation of composites and the interaction of MoS_2, h-BN, and TiO_2 with PANI matrix and GO for corresponding composite samples. These results are consistent with the previous report for the synthesis of ternary composites by the addition of metal oxides with the polymer [20].

3.2. X-ray diffraction analysis (XRD)

The X-ray diffraction (XRD) patterns of PANI, GO, PANI/GO, PANI/GO/MoS_2, PANI/GO/h-BN, PANI/GO/TiO_2 nanocomposites are shown in Fig. 2. The X-ray diffraction pattern of polyaniline in Fig. 2 (a) indicates that it is semi-crystalline, with a broad peak centered about 2 theta =26°. Moreover, the diffraction peaks at 2θ equals 9.27^0, 20° and

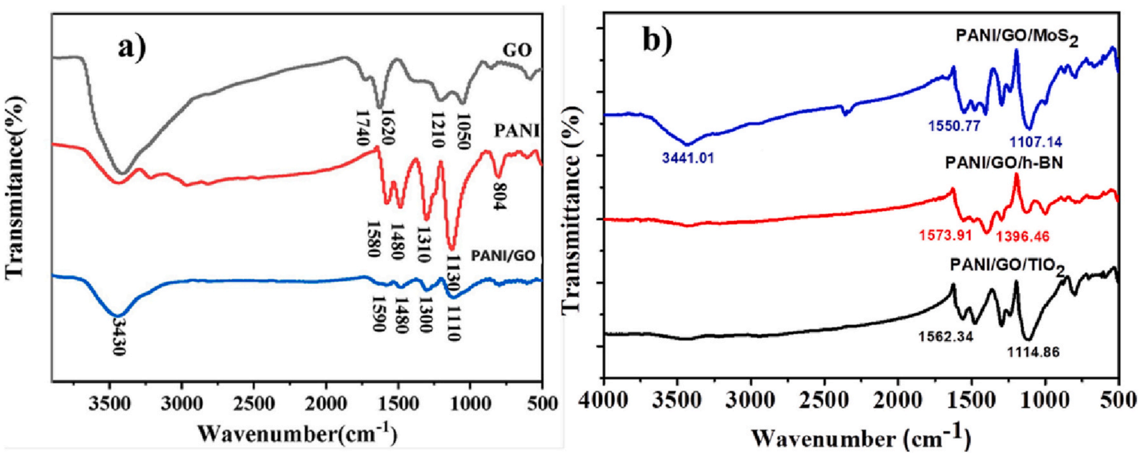

Fig. 1. FTIR of PANI, GO and PANI/GO (a), and PANI/GO/MoS$_2$, PANI/GO/h-BN, and PANI/GO/TiO$_2$ nanocomposites (b).

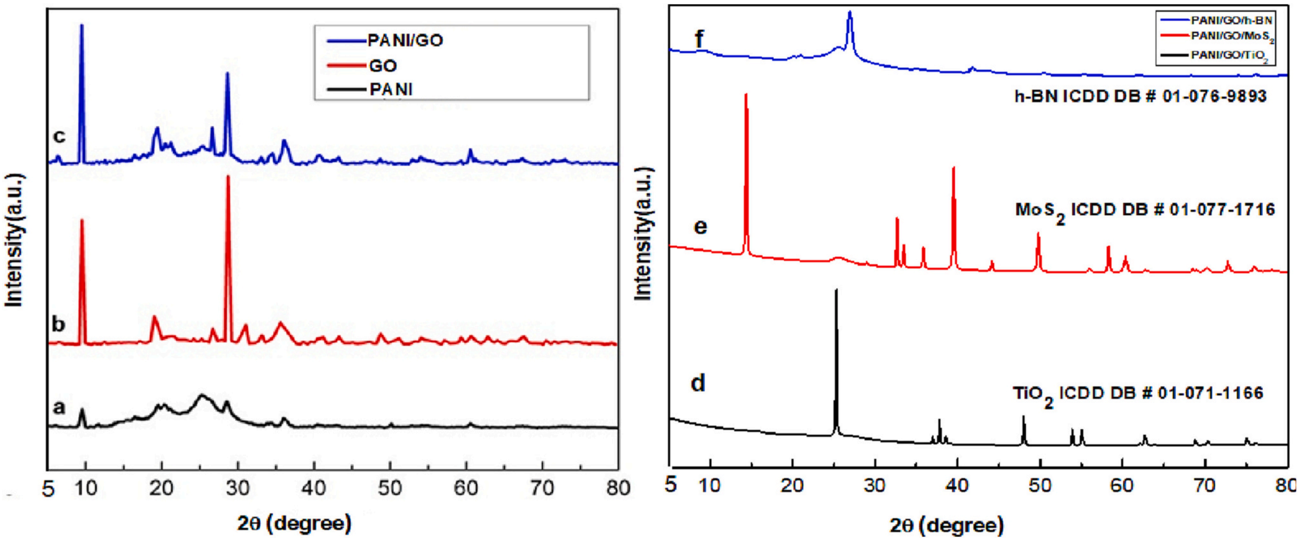

Fig. 2. XRD of (a) PANI, (b) GO, (c) PANI/GO, (d) PANI/GO/TIO$_2$, (e) PANI/GO/MoS$_2$ and (f) PANI/GO/h-BN.

29° supports the ordered crystal structure of PANI, which may improve the crystallinity of the composite considerably, because of the presence of benzenoid and quinonoid group in the Polyaniline. These results are consistent with the previous report on the XRD pattern of PANI [20]. The XRD pattern of GO as presented in Fig. 2(b), $2\theta = 10^\circ$ corresponds to the (001) reflection with an average d-spacing of around 0.79 nm, and the $2\theta = 31^o$ and 37^o confirm the parent graphite's layered structure. These results can be attributed to the insertion of oxygen-containing functional groups on the pristine graphite. Fig. 2(c) depicts the XRD pattern of a PANI/GO composites. The structure of GO has been validated by comparing the XRD patterns of the composites and GO, despite the fact that it was dispersed in PANI during the polymerization operation. It may be inferred from Fig. 2 that the peak height of the GO planes decreases in the composites might be caused by the incorporation of GO in the PANI matrix.

Fig. 2 (d, e and f) represents the XRD patterns of PANI/GO/TiO$_2$, PANI/GO/MoS$_2$, and PANI/GO/h-BN, nanocomposites. The diffraction pattern of PANI/GO/MoS$_2$ demonstrates intense peaks at $2\theta = 12^o$ and 40^o. For PANI/GO/h-BN and PANI/GO/TiO$_2$, the major peaks were identified at $2\theta = 28^o$ and 26^o, respectively. It is clear that the peak position (2θ) and intensity of composite samples of PANI/GO/h-BN, PANI/GO/MoS$_2$ and PANI/GO/TiO$_2$ has reformed compared to PANI due to incorporation of amorphous carbon by h-BN, MoS$_2$ and TiO$_2$, respectively. This modification may be the reason for enhancement in better charge storage capacity exhibited by the composites. Besides, for PANI/GO/h-BN composites the peak $2\theta = 28^o$ shifted from 26^o (for PANI), and 31^o (for GO) indicates good interaction between PANI, GO and h-BN. This kind of interaction can be attributed to the fact that highly crystalline h-BN has been compounded with amorphous PANI and GO resulting in the shifting of peak.

Crystalline size of the prepared nanocomposites has been calculated from the X-ray diffraction and presented in Table 1. It is notable that PANI/GO/h-BN nanocomposite shows larger crystalline coherence length (L), indicating its better charge transfer capacity along the chain [21]. In addition, PANI/GO/h-BN nanocomposite demonstrates shorter interchain separation length (R) which promotes conductivity as the hopping distance of electrons from one chain to another decreases [21].

3.3. SEM analysis

Fig. 3(a-e) presents the SEM images of the PANI, PANI/GO, PANI/GO/h-BN, PANI/GO/MoS$_2$ and PANI/GO/TiO$_2$ nanocomposites which exhibit different morphologies. Fig. 3a demonstrates aggregated particle of PANI, while Fig. 3b shows morphology of PANI/GO which indicates few layers of GO stacked on PANI slackly and are rumbled like a silken veil, which may be explained by the π-π stacking between GO [20]. The Fig. 3(b-e) evidences porous structure of PANI/GO, PANI/GO/h-BN, PANI/GO/MoS$_2$ and PANI/GO/TiO$_2$ which may be attributed by the

Table 1
Crystalline size of different electrodes.

Sample	Cu Source, λ (Å)	2θ	Full width with half maximum, β	Interlayer Spacing, d	$L() = \frac{0.89\lambda}{\beta cos\theta}$	$R(Å) = \frac{5\lambda}{8sin\theta}$
PANI/GO	1.54	26.61	0.11	3.3475	6.08	4.19
PANI/GO/h-BN		26.93	0.60	3.3079	12.37	4.14
PANI/GO/MoS_2		14.38	0.20	6.1537	6.80	7.70
PANI/GO/TiO_2		25.3	0.11	3.5175	12.0	4.40

presence of GO in the nanocomposite. The porous structure of PANI/GO based ternary nanocomposite may contribute to the electrochemical properties of the materials.

3.4. Thermogravimetric analysis

TGA thermograms of PANI, PANI/GO, PANI/GO/h-BN, PANI/GO/MoS_2 and PANI/GO/TiO_2 are presented in Fig. 4. The Figure shows that decomposition of PANI started at 130 °C, while PANI/GO nanocomposite shows three major stages of weight loss. The first stage of weight loss was found about 12 % at 188 °C due to moisture loss, another 15 % weight loss was found in the second stage at 253 °C due to removal of low molecular weight oligomer, and finally decomposition took place in the temperature range of 370–700 °C which led to a weight loss of about 22 %. The thermogram of PANI/GO clearly indicates improvement in thermal stability and decomposition temperature, and this increment is attributed to the GO. Similarly, thermograms of the PANI/GO/h-BN, PANI/GO/MoS_2 and PANI/GO/TiO_2 nanocomposite shows the improved thermal properties, and this improvement is contributed by the h-BN and metal oxides.

3.5. Electrochemical properties

Fig. 5 presents the variation in I-V (Current vs Voltage) curve of PANI/GO, PANI/GO/h-BN, PANI/GO/MoS_2 and PANI/GO/TiO_2 nanocomposites at different scan rate ranging from 10 mV/s to 50 mV/s. The

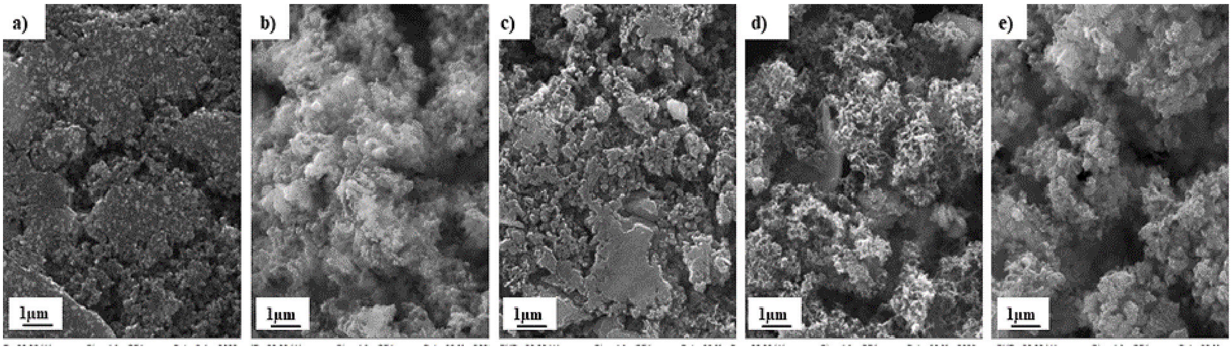

Fig. 3. SEM images of PANI (a), PANI/GO (b), PANI/GO/h-BN (c), PANI/GO/MoS_2 (d) and PANI/GO/TiO_2 nanocomposites (e).

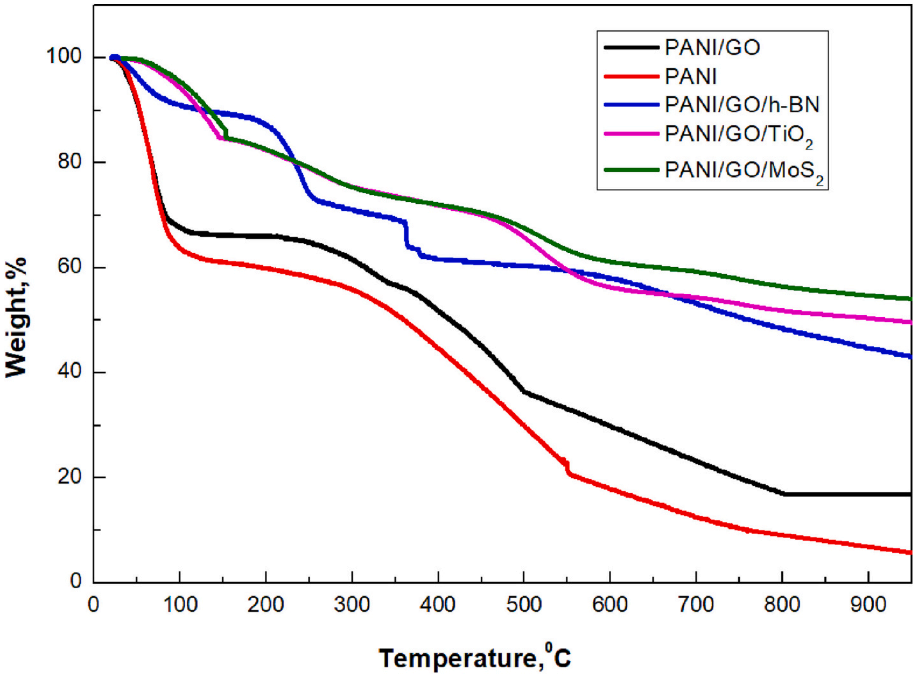

Fig. 4. TGA thermograms of PANI, PANI/GO, PANI/GO/h-BN and PANI/GO/TiO_2.

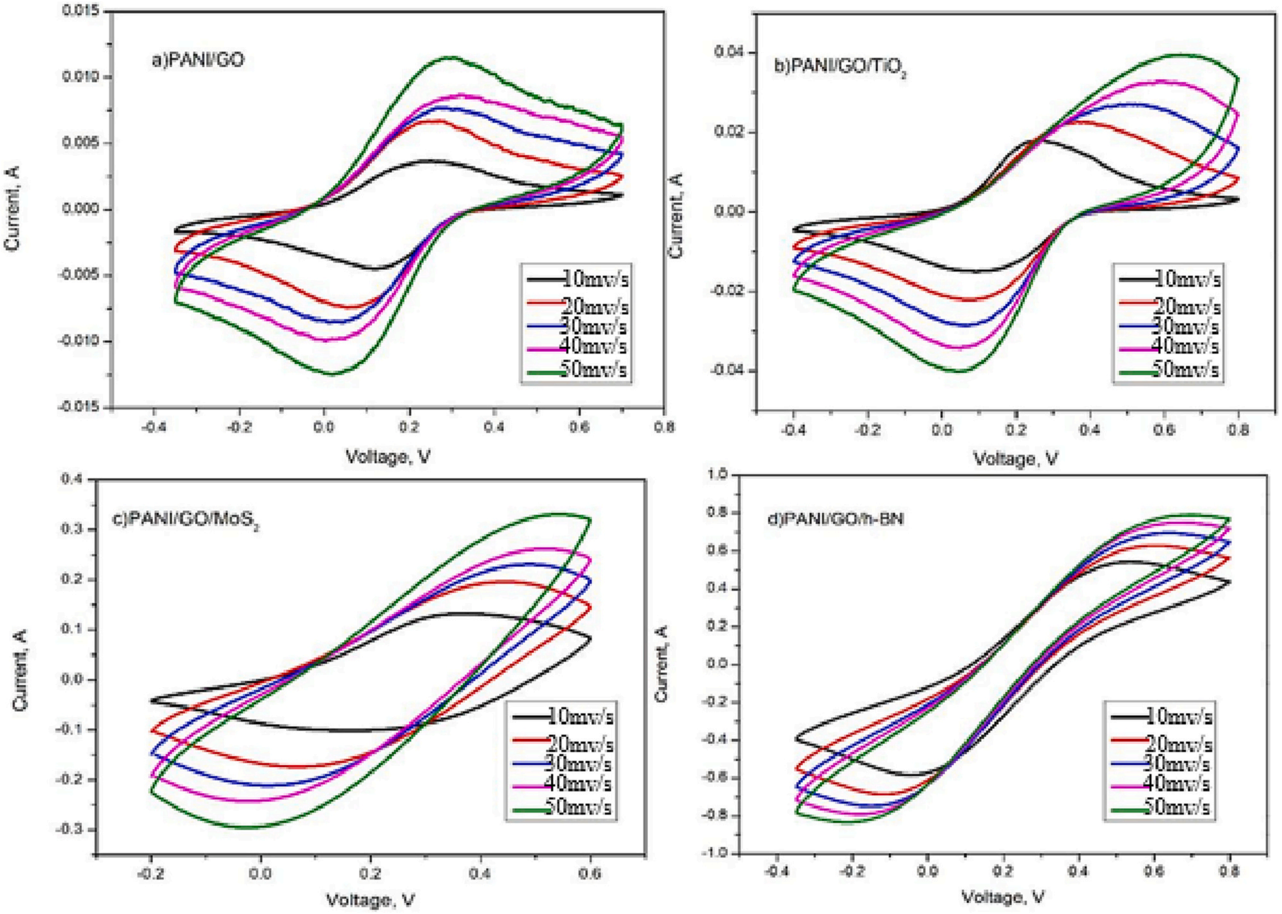

Fig. 5. Cyclic voltammetry of PANI/GO (a). PANI/GO/h-BN (b), PANI/GO/TiO$_2$ (c) and PANI/GO/MoS$_2$ (d) nanocomposites at various scan rate (mV/s) against Ag/AgCl reference electrode and 1 M Na$_2$SO$_4$ electrolyte.

figures show an ideal characteristic CV profile at a lower scan rate of 10 mV/s (Fig. 4a-d), indicating formation of double layer capacitance at the surface [13]. The figure clearly demonstrates that incorporation of graphene oxide, h-BN, MoS$_2$ and TiO$_2$ with PANI improves the charge storage capacity, thus the composites retain ideal rectangular shaped CV even at a higher scan rate.

Variation of specific capacitance with different scan rate is presented in Fig. 6(a). Fig. 6(a) shows that the specific capacitance of the PANI/GO nanocomposites decreases with increasing scan rate. The lower capacitance can be explained by the existence of inner active sites, which are unable to completely maintain redox transitions at higher scan rates. PANI/GO nanocomposites exhibited capacitance of 665 F/g and 204 F/g at the scan rate of 10 mV/s and 50 mV/s, respectively. PANI/GO nanocomposites showed higher specific capacitance compared to PANI at any scan rate. In a PANI/GO nanocomposites, graphene oxide is acidic group, remains conductive for a long time and no migration occurs in composites, in addition GO and PANI exhibit synergistic effects in PANI/GO composites, GO and PANI provides flexibility and electroactivity, respectively in electronic devices [10].

Among different ternary nanocomposites prepared in this study, PANI/GO/h-BN shows the highest specific capacitance of 946 F/g at 10 mV/s scan rate and 226 F/g at 50 mV/s scan rate. This increment in capacitance of PANI/GO/h-BN is totally contributed by the synergistic effect of GO and h-BN. GO has the potential for the synthesis of functional nanocomposites because of its adaptable oxygen functional groups and strong compatibility with polymers. PANI and GO work together synergistically to improve the electroactivity of PANI/GO composites. Incorporation of h-BN improves the attraction between anilinium cations (phenyl-NH^{+3}) and surface of h-BN that results enhancement of capacitance of the PANI/GO/h-BN composite coulombic among anilinium cations and the h-BN surface. This better performance of PANI/GO/h-BN is also supported by the impedance spectrum. Similarly, PANI/GO-MoS$_2$ and PANI/GO-TiO$_2$ show 815 F/g and 713 F/g at 10 mV/s, respectively.

Variations of energy density of PANI, PANI/GO, PANI/GO/h-BN, PANI/GO/TiO$_2$ and PANI/GO/MoS$_2$ nanocomposites as a function of scan rate are demonstrated in Fig. 6(b). Similar to specific capacitance, Fig. 6(b) shows that Energy density of all the composites decreased with the increasing scan rate. In the case of PANI, energy density decreased from 90 Wh/kg at 10 mV/s to 13 Wh/kg at 50 mV/s. PANI/ GO/h-BN exhibited energy density as high as 624 Wh/kg at the scan rate of 10 mV/s and 129 Wh/kg at 50 mV/s. However, Fig. 6(c) shows that the power density of PANI, PANI/GO, PANI/GO/h-BN, PANI/GO/TiO$_2$ and PANI/GO/MoS$_2$ nanocomposites increases with scan rate. PANI/GO/TiO$_2$ exhibited the highest power density of 5828 W/kg, and PANI/GO/MoS$_2$ nanocomposites demonstrated 5087 W/kg at the scan rate of 50 mV/s.

Capacitive retention of PANI and its nanocomposite after 100 cycles of charge-discharge is presented in Fig. 6(d). PANI/GO/h-BN nanocomposite exhibited highest cyclic retention (98 %) among other prepared composite in this study.

Fig. 7 shows the comparative GCD curve of PANI/GO, PANI/GO/h-BN, PANI/GO/MoS$_2$ and PANI/GO/TiO$_2$ nanocomposites. PANI/GO/h-BN shows the lowest voltage difference which clearly indicates better capacitance of the electrode (according to Eq. (1)). It also demonstrates higher discharge time compared to other electrodes.

On the other hand, variation of dielectric properties of the prepared nanocomposites electrodes as a function of frequency is presented in

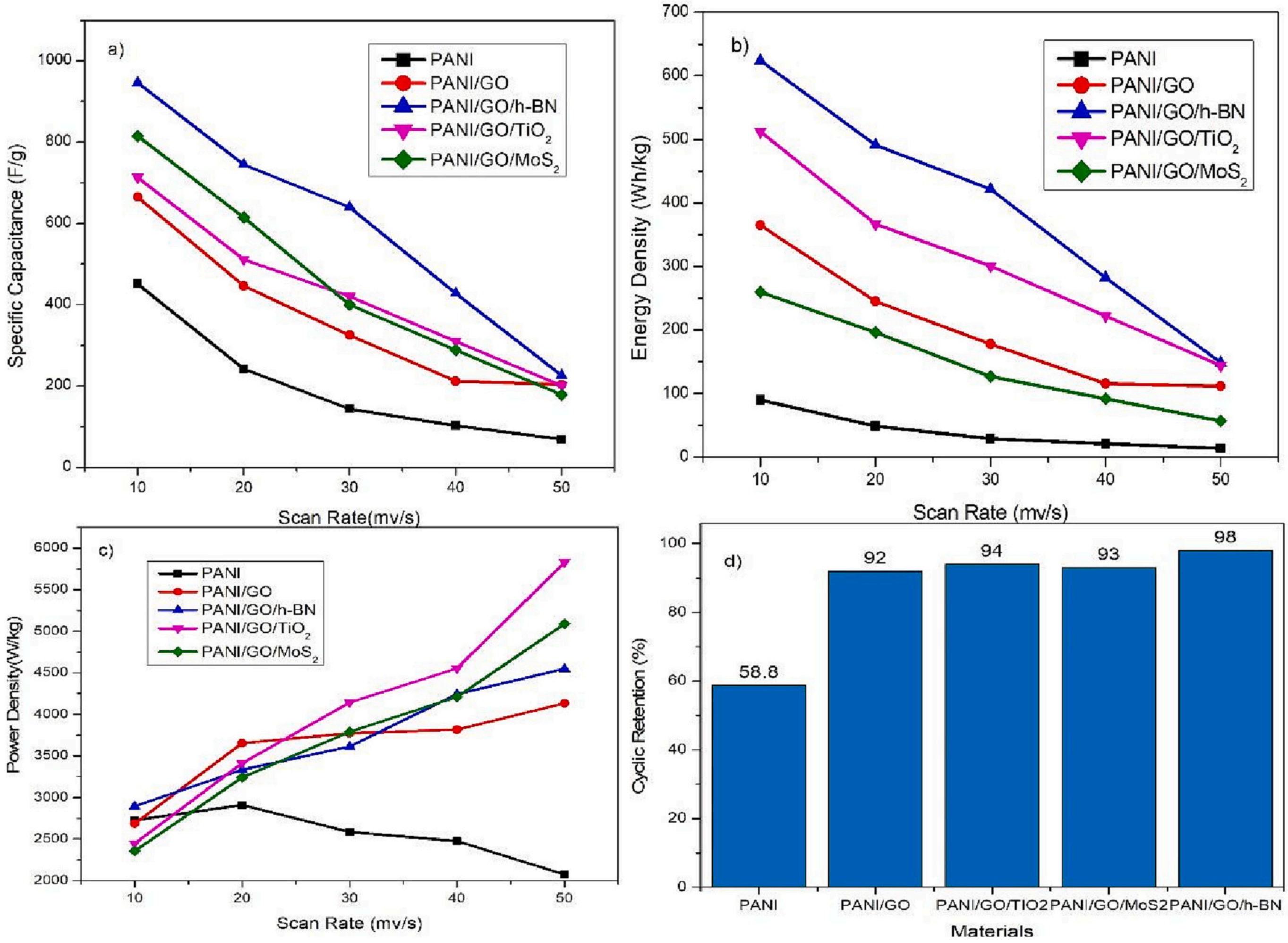

Fig. 6. Variation of specific capacitance (a), energy density (b), power density(c) and cyclic retention (d) of PANI, PANI/GO, PANI/GO/h-BN, PANI/GO/MoS_2 and PANI/GO/TiO_2 nanocomposites with different scan rates (mV/s).

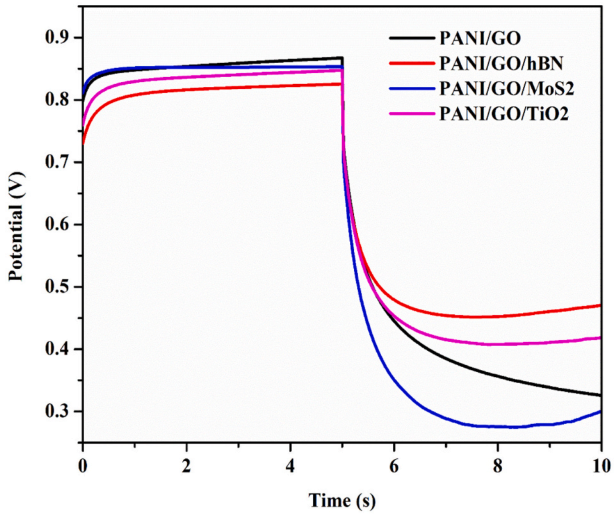

Fig. 7. GCD curve of PANI/GO, PANI/GO/h-BN, PANI/GO/MoS_2 and PANI/GO/TiO_2 nanocomposites at 1 mA/cm^2.

Fig. 8(a). Fig. 8(a) shows the least dielectric loss for PANI/GO/h-BN electrodes compared to other electrodes which clearly supports the better energy storage capacity of the electrode. Fig. 8(b) presents the Cole-Cole plot of the prepared electrodes at room temperature. From the figure, it is possible to notice that the grain size of PANI/GO/h-BN is greater than that of the others, which clearly indicates better energy storage capacity of the PANI/GO/h-BN electrode compared to others, it also supports the findings by the CV study.

A comparison of electrochemical performances of electrodes developed in this study (PANI/GO, PANI/GO/h-BN, PANI/GO/MoS_2 and PANI/GO/TiO_2 nanocomposites), and the similar electrode materials reported in the literature are presented in the Table 2. In our study, PANI/GO/h-BN nanocomposite shows the highest sp. capacitance of 946 F/g at 10 mV/s compared to other electrodes. While, in the literature, Aziz et al. reported that nitrogen doped GO (NGO)-based NGO/$NiWO_3$/PANI electrode showed maximum sp. capacitance of 1380 F/g, better electrochemical properties may be contributed by the Nickel tungstate. In our previous study, it was found that PANI/h-BN demonstrated sp. capacitance as high as 927 F/g [27], on the other hand PANI exhibited sp. capacitance of only 451 F/g. It is noticeable that incorporation of GO and h-BN with PANI significantly improved energy storage capacity. In the literature, most of the studies showed energy density as a function of power density, but this study showed that energy density also varied with scan rate as presented in Fig. 5(c). Our developed PANI/GO/h-BN also yielded better energy density and cyclic retention compared to other electrodes reported in the literature.

Performance of electrode material for supercapacitors is commonly affected by the corrosion on current collectors. Thus, the corrosion phenomena on current collectors due to electrochemical action of the

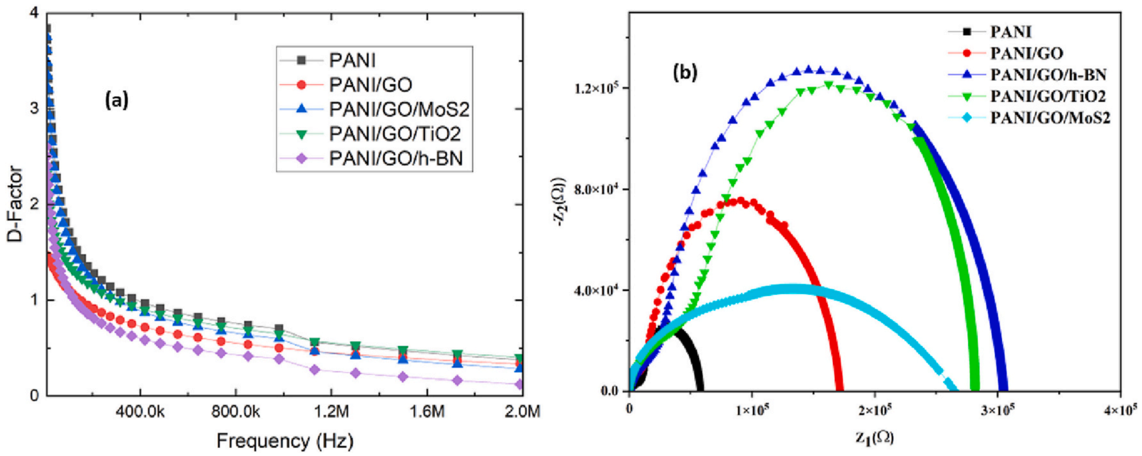

Fig. 8. (a) Variation of Dissipation-Factor with frequency and (b) Cole-Cole plots with interpolation.

Table 2
Comparison in electrochemical performance of PANI/GO-based electrode.

Electrode	Sp. Capacitance at different scan rate or current density	Cyclic Retention	Energy Density at Different Power Density	Reference
SnO_2/RGO@PANI	366.30 F/g at 1 A/g	88 % after 50 cycles	147.92 Wh/kg	[23]
NGO/$NiWO_3$/PANI	1380 F/g at 0.5 A/g	92.6 % after 10,000 cycles	47.8 Wh/kg	[24]
$Ti_3C_2T_X$ @PANI-RGO	617.84 F/g at 0.5 A/g	92.52 % after 10,000 cycles	269.18 Wh/kg at 527.72 W/kg	[25]
PANI/GO/$CuFe_2O_4$	614.76 F/g at 1 A/g	88 % after 3500 cycles	–	[26]
PANI/h-BN	927 F/g at 10 mV/s	97.6 % after 100 cycles	120 Wh/kg at 4405 W/kg	[27]
PANI/CdO/GO	647 F/g at 1 A/g	82 % after 500 cycles	116.6 Wh/kg at 388 W/kg	[28]
Fe_3O_4@Fc-GO/PANI	640 mAh/g at 1 A/g	86.68 % after 5000 cycles	–	[29]
GO-Fc/PANI	208 mAh/g at 2.5 A/g	85.54 % after 3000 cycles	–	[30]
PANI	451 F/g at 10 mV/s	58.8 % after 100 cycles	90 Wh/kg at 2727 W/kg	This Work
PANI/GO	665 F/g at 10 mV/s	92 % after 100 cycles	365 Wh/kg at 2684 W/kg	This Work
PANI/GO/h-BN	946 F/g at 10 mV/s	98 % after 100 cycles	624 Wh/kg at 2894 W/kg	This Work
PANI/GO/MoS_2	815 F/g at 10 mV/s	93 % after 100 cycles	260 Wh/kg at 2356 W/kg	This Work
PANI/GO/TiO_2	713 F/g at 10 mV/s	94 % after 100 cycles	512 Wh/kg at 2446 W/kg	This Work

electrode materials during charging-discharging were studied by electrochemical polarization method using three electrode systems in 1 M Na_2SO_4 solution. Tafel extrapolation showed less corrosion rate and smaller corrosion current for PANI/GO/h-BN electrode compared to other electrodes (Table 3), which indicates better anti-corrosion property that led to better stability of the current collector in a supercapacitor cell [22].

3.6. Performance of asymmetric supercapacitor

The performance of the supercapacitor was evaluated following GCD technique. Table 4 shows that the supercapacitor with PANI/GO/h-BN composite as electrode material exhibited highest capacitance compared to the supercapacitor with PANI or other electrodes. PANI/GO/h-BN//AC device exhibited maximum capacitance of 351.43 F/g, energy density of 25.7 Wh/kg, power density of 1335 W/kg and cyclic retention of 53.80 % after 50 cycles. While PANI demonstrates specific Capacitance of 203 F/g, energy density of 22 Wh/kg, power density of 1215 and cyclic retention of 38 %. Improvement of specific capacitance for PANI/GO/h-BN composite is contributed by GO and h-BN, and the reason is explained in the previous paragraph with supporting reference.

Table 3
Tafel extrapolation data at 10 mV/s.

Electrode	I_{corr} (Amp/cm^2)	Corrosion Rate (MPY)
PANI/GO	7.47E-03	1.48E-02
PANI/GO/h-BN	1.38E-03	4.71E-03
PANI/GO/MoS_2	1.68E-03	3.34E-02
PANI/GO/TiO_2	1.57E-03	1.56E-02

Table 4
Electrical properties of ASD prepared with various electrode materials.

Cathode materials along with Co_3O_4 and APS	Capacitance (F/g)	Energy density (Wh/kg)	Power density (W/kg)	Cyclic retention (%)
PANI	203	22	1215	38
PANI/GO	222	23	1368	56.18
PANI/GO/TiO_2	341.94	25.34	1256	43.80
PANI/GO/h-BN	351.43	25.7	1335	53.80
PANI/GO/MoS_2	288.35	18.16	1050	21.71

Variation of potential as a function of discharge time at constant current is presented in the Fig. 9. This figure shows that PANI/GO/TiO_2//AC supercapacitor device exhibits longer discharge time compared to that with other electrode materials.

Finally, to demonstrate a real application, the real asymmetric supercapacitor device constructed with the ternary nanocomposite prepared in this study (PANI/GO/h-BN//AC and PANI/h-BN//AC) was connected in parallel with an LED as shown in Fig. S2(see supplementary figure). The device was charged for 120 s at 5 V using a DC power supply, then a 5 mm LED bulb was connected for discharging, and it was lit up. The LED was utilized to monitor the response of the supercapacitor device. Table 5 shows the charging and discharging time with maximum attained voltage for different electrodes. PANI/GO/h-BN//AC device shows highest discharge time, it lit up a green 5 mm LED as much as 243 min from only 20 min charging. It also attained the highest voltage (4.7 V). Hence, the potentiostatic, galvanostatic and real device application clearly showed the better performance of PANI/h-BN//AC, and the electrode material can be effectively employed to fabricate

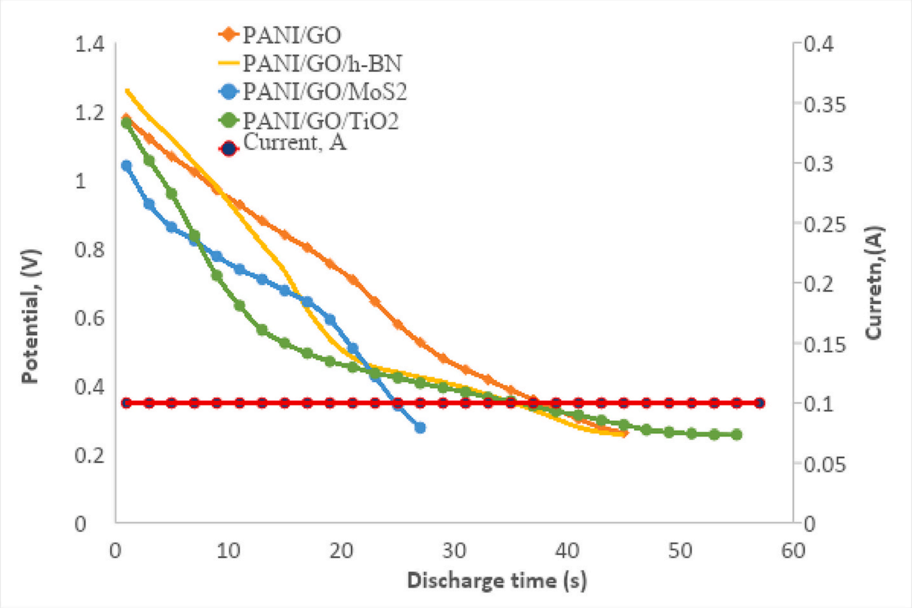

Fig. 9. Variation of potential as a function of discharge time at constant current for different cathode materials.

highly efficient next generation supercapacitors.

Table 5
Performance of ASD prepared with various electrode materials.

Electrode	Charging time, min	Discharging time, min	Max. attained Voltage, V	I, mA
PANI	20	47	3	0.5
PANI/GO	20	240	4.7	1
PANI/GO/h-BN	20	243	3.7	0.5
PANI/GO/TiO_2	20	239	3.6	0.7
PANI/GO/MoS_2	20	50	3.4	0.6

4. Conclusion

In this study, PANI/GO, PANI/GO/TiO_2, PANI/GO/MoS_2 and PANI/GO/h-BN ternary nanocomposites were synthesized successfully and characterized systematically. TGA shows that incorporation of GO and boron compound improves thermal stability of PANI based nanocomposite. CV study shows that incorporation of GO in the PANI matrix improved electrochemical properties, and PANI/GO/h-BN nanocomposite demonstrated highest specific capacitance of 946 F/g and energy density of 624 Wh/kg among other PANI/GO based ternary nanocomposites. Furthermore, impedance spectrum analysis (Cole-Cole diagram) showed greater grain size of the PANI/GO/h-BN, indicating higher energy storage capacity of the electrode which supports the results found in the CV study. It was found that all the nanocomposites with metal oxides and sulfide exhibited better electrochemical properties at lower scan rates. Additionally, Tafel extrapolation indicated the PANI/GO/h-BN electrode showed less corrosion compared to other electrodes. Considering the excellent electrochemical properties of PANI/GO based nanocomposite, a set of asymmetric hybrid supercapacitors were constructed using the prepared nanocomposite as a positive electrode. The performance of the supercapacitor was evaluated by galvanostatic charge-discharge technique. It was found that the PANI/GO/h-BN//AC supercapacitor device exhibited the highest specific capacitance (351 F/g), energy density, and power density, compared to the supercapacitors with other nanocomposites. Finally, results obtained from all the three configurations (potentiostatic, galvanostatic and real device performance) show that PANI/GO/h-BN and PANI/GO/TiO_2 nanocomposites have very good prospects as electrode materials for a highly efficient supercapacitor.

CRediT authorship contribution statement

Md Mostafizur Rahman: Conceptualization, Data curation, Supervision, Writing - review and editing, Funding acquisition, Project administration. **Minhazur Rahman Whawon**: Synthesis, Methodology, Writing - original draft. **Md Habibur Rahman**: Construction of asymmetric supercapacitor, Formal analysis, Data curation, draft writing. **Md Iftidul Alam**: Data curation, Investigation, Writing - original draft. **Omar Faruk:** XRD and impedance analysis. **Mohammad Mizanur Rahman Khan**: FTIR analysis, Review and editing. **Okenwa Okoli**: Review and editing.

Declaration of competing interest

Data availability

The raw/processed data required to reproduce these findings cannot be shared at this time as the data also forms part of an ongoing study. But data will be available on request.

Acknowledgment

This work is completely conducted in the laboratory of the Department of Chemical Engineering and Polymer science, SUST. This study was financially supported by the Grant for Advanced Research in Education, the Ministry of Education, Government of the People's Republic of Bangladesh (Research grant July 2020-June 2023, Project code: PS20191250). We also acknowledge grants from SUST research center (AS/2021/1/09).

Appendix A. Supplementary data

Supplementary data to this article can be found online at https://doi.org/10.1016/j.est.2023.107615.

References

[1] F.M.Mohd Omaish Ansari, Thermal stability, electrical conductivity and ammonia sensing studies on P-toluenesulfonic acid doped polyaniline:titanium dioxide (pTSA/Pani:TiO2) nanocomposites, Sensors Actuators B Chem. 157 (2011) 122–129, https://doi.org/10.1016/j.snb.2011.03.036.

[2] K.S. Ryu, K.M. Kim, N.G. Park, Y.J. Park, S.H. Chang, Symmetric redox supercapacitor with conducting polyaniline electrodes, J. Power Sources 103 (2002) 305–309, https://doi.org/10.1016/S0378-7753(01)00862-X.

[3] S. Ghosh, T. Maiyalagan, R.N. Basu, Nanostructured conducting polymers for energy applications: towards a sustainable platform, Nanoscale 8 (2016) 6921–6947, https://doi.org/10.1039/c5nr08803h.

[4] R. Ramachandran, S.M. Chen, G.Gnana Kumar, An overview of electrochemical energy storage devices of various electrodes and morphological studies of supercapacitors, Int. J. Electrochem. Sci. 10 (2015) 10355–10388.

[5] W. Yoon, S. Lee, Polypyrrole nanotubes conjugated with human olfactory receptors: high-performance transducers for FET-type bioelectronic noses, Angew. Chem. Int. Ed. 48 (2009) 2755–2758, https://doi.org/10.1002/anie.200805171.

[6] R.K. Sharma, A.C. Rastogi, S.B. Desu, Manganese oxide embedded polypyrrole nanocomposites for electrochemical supercapacitor, Electrochim. Acta 53 (2008) 7690–7695, https://doi.org/10.1016/j.electacta.2008.04.028.

[7] M. Rahman, T. Mahtab, M.Z. Bin Mukhlish, M.O. Faruk, M.M. Rahman, Enhancement of electrical properties of metal doped polyaniline synthesized by different doping techniques, Polym. Bull. (2020), https://doi.org/10.1007/s00289-020-03389-9.

[8] S.M. Chen, R. Ramachandran, V. Mani, R. Saraswathi, Recent advancements in electrode materials for the high-performance electrochemical supercapacitors: a review, Int. J. Electrochem. Sci. 9 (2014) 4072–4085.

[9] P.S.S. Sagadevan, I. Das, K. Pal, P. Murugasen, Optical and electrical smart response of chemically stabilized graphene oxide, J. Mater. Sci. Electron. 28 (2017) 5235–5243.

[10] X. Wang, H. Hao, Q. Yang, L.X. Lu, Wang, Graphene oxide doped polyaniline for supercapacitors, Electrochem. Commun. 11 (2009) 1158–1161, https://doi.org/10.1016/J.ELECOM.2009.03.036.

[11] J.W.K. Zhang, L. Zhang, X. Zhao, Graphene/polyaniline nanofiber composites as supercapacitor electrodes, Chem. Mater. 22 (2010) 1392–1401.

[12] J.W.L. Mao, K. Zhang, H.S. On Chan, Surfactant-stabilized graphene/polyaniline nanofiber composites for high performance supercapacitor electrode, J. Mater. Chem. 22 (2012) 80–85.

[13] T. Wang, H. Sun, T. Peng, B. Liu, Y. Hou, B. Lei, Preparation and characterization of polyaniline/p-phenylenediamine grafted graphene oxide composites for supercapacitors, J. Mol. Struct. 1221 (2020), 128835, https://doi.org/10.1016/j.molstruc.2020.128835.

[14] S. Zhou, H. Zhang, Q. Zhao, X. Wang, J. Li, F. Wang, Graphene-wrapped polyaniline nanofibers as electrode materials for organic supercapacitors, Carbon N. Y. 52 (2013) 440–450, https://doi.org/10.1016/j.carbon.2012.09.055.

[15] W.F.Q. Zhang, Y. Li, Y. Feng, Electropolymerization of graphene oxide/ polyaniline composite for high-performance supercapacitor, Electrochim. Acta 90 (2013) 95–100.

[16] M.M. Rahman, P.M. Joy, M.N. Uddin, M.Z. Bin Mukhlish, M.M.R. Khan, Improvement of capacitive performance of polyaniline based hybrid supercapacitor, Heliyon 7 (2021), https://doi.org/10.1016/j.heliyon.2021.e07407.

[17] P. Liu, J. Yan, Z. Guang, Y. Huang, X. Li, W. Huang, Recent advancements of polyaniline-based nanocomposites for supercapacitors, J. Power Sources 424 (2019) 108–130, https://doi.org/10.1016/j.jpowsour.2019.03.094.

[19] W. Yang, P. Mai, Flexible solid-state electrochemical supercapacitors, Nano Energy 8 (2014) 274–290.

[20] A.H. Gemeay, R.G. Elsharkawy, E.F. Aboelfetoh, Graphene oxide/polyaniline/manganese oxide ternary nanocomposites, facile synthesis, characterization, and application for indigo carmine removal, J. Polym. Environ. 26 (2018) 655–669, https://doi.org/10.1007/s10924-017-0947-z.

[21] S.M.X. Du, Y. Xu, L. Xiong, Y. Bai, J. Zhu, Polyaniline with high crystallinity degree: synthesis, structure, and electrochemical properties, J. Appl. Polym. Sci. (2014), https://doi.org/10.1002/app.40827.

[22] A.E.K. Kakaei, M.D. Esrafili, Chapter 8 - Graphene and Anticorrosive Properties, Elsevier, 2019, https://doi.org/10.1016/B978-0-12-814523-4.00008-3.

[23] D. Bejjanki, G.U.B. Babu, K. Kumar, S.K. Puttapati, SnO2/RGO@PANi ternary composite via chemical oxidation polymerization and its synergetic effect for better performance of supercapacitor, Mater. Today: Proc. (2023), https://doi.org/10.1016/j.matpr.2022.11.199.

[24] M.H. Aziz, F. Shaheen, R. Ahmad, A. Khan, S. Sharif, H.M. Fahad, Q. Huang, Facile hydrothermal synthesis of NGO/NiWO3/PANI nanocomposite for durable and high-performance hybrid supercapacitors, Mater. Lett. (2023), https://doi.org/10.1016/j.matlet.2022.133658.

[25] P. Liao, Y. Zeng, Z. Qiu, S. Hao, J. He, H. Xu, S. Chen, 3D Ti3C2TX@PANI-reduced graphene oxide hydrogel and defective reduced graphene oxide hydrogel as anode and cathode for high-energy asymmetric supercapacitor, J. Alloys Compd. (2023), https://doi.org/10.1016/j.jallcom.2023.169593.

[26] A.K. Ghasemi, M. Ghorbani, M.S. Lashkenari, N. Nasiri, Facile synthesize of PANI/GO/CuFe2O4 nanocomposite material with synergistic effect for superb performance supercapacitor, Electrochim. Acta (2023), https://doi.org/10.1016/j.electacta.2022.141685.

[27] M.M. Rahman, M.R. Hossen, I. Alam, M.H. Rahman, O. Faruk, M. Nurbas, M. M. Rahman, M.M.R. Khan, Synthesis of hexagonal boron nitride based PANI/h-BN and PANI-PPy/hBN nanocomposites for efficient supercapacitors, J. Alloys Compd. (2023), https://doi.org/10.1016/j.jallcom.2023.169471.

[28] A.G. Kenesi, M. Ghorbani, M.S. Lashkenari, High electrochemical performance of PANI/CdO nanocomposite based on graphene oxide as a hybrid electrode material for supercapacitor application, Int. J. Hydrog. Energy (2022), https://doi.org/10.1016/j.ijhydene.2022.09.047.

[29] E. Payami, R.T. Mofrad, A novel ternary Fe3O4@Fc-GO/PANI nanocomposite for outstanding supercapacitor performance, Electrochim. Acta (2021), https://doi.org/10.1016/j.electacta.2021.138296.

[30] R.T. Mofrad, E. Payami, I. Ahadzadeh, Synthesis, characterization, and electrochemical evaluation of a novel high-performance GO-Fc/PANI nanocomposite for supercapacitor applications, Electrochim. Acta (2019), https://doi.org/10.1016/j.electacta.2019.134706.